Chapter 20

Quantifying Force and Viscoelasticity Inside Living Cells Using an Active–Passive Calibrated Optical Trap

Christine M. Ritter, Josep Mas, Lene Oddershede, and Kirstine Berg-Sørensen

Abstract

As described in the previous chapters, optical tweezers have become a tool of precision for in vitro single-molecule investigations, where the single molecule of interest most often is studied in purified form in an experimental assay with a well-controlled fluidic environment. A well-controlled fluidic environment implies that the physical properties of the liquid, most notably the viscosity, are known and the fluidic environment can, for calibrational purposes, be treated as a simple liquid.

In vivo, however, optical tweezers have primarily been used as a tool of manipulation and not so often for precise quantitative force measurements, due to the unknown value of the spring constant of the optical trap formed within the cell's viscoelastic cytoplasm. Here, we describe a method for utilizing optical tweezers for quantitative in vivo force measurements. The experimental protocol and the protocol for data analysis rely on two types of experiments, passive observation of the thermal motion of a trapped object inside a living cell, followed by observations of the response of the trapped object when subject to controlled oscillations of the optical trap. One advantage of this calibration method is that the size and refractive properties of the trapped object and the viscoelastic properties of its environment need not be known. We explain the protocol and demonstrate its use with experiments of trapped granules inside live *S. pombe* cells.

Key words Optical tweezers, Viscoelasticity, Cytoplasm, In vivo, Force measurements, Spring constant

1 Introduction

Optical tweezers have been widely used in the field of biophysics in the past decades to perform quantitative force measurements on biomolecules [1–4]. Most of these force measurements were performed in vitro, where the experimental conditions can be controlled. Sophisticated calibration procedures for in vitro experiments, where the object of interest is in a purely viscous environment, have been developed [5–8]. One standard procedure is the power spectrum analysis [5]. In this calibration procedure,

Arne Gennerich (ed.), *Optical Tweezers: Methods and Protocols*, Methods in Molecular Biology, vol. 1486, DOI 10.1007/978-1-4939-6421-5_20,

the Brownian motion of a particle trapped in the quasi-harmonic potential of optical tweezers is interpreted by its power spectrum.

In vitro measurements of single molecules have given us a better understanding of how these molecules work. To get an even better understanding of their role within the cell, measurements in the natural environment of these molecules are necessary [9–13]. Optical tweezers can be used to trap organelles or internalized handles inside living cells or even entire cells without disrupting the cell wall [14–17]. Choosing an infrared or near-infrared laser for the optical tweezers can minimize the amount of energy deposited in a cell which reduces physiological damage and the effect of heating [18–20]. Other commonly used techniques for in vivo measurements are atomic force microscopy [21] and magnetic tweezers [22]. Atomic force microscopy, however, cannot reach within the cell without penetrating the cell wall and magnetic tweezers rely on the internalization of magnetic handles whereas optical tweezers can trap endogenous objects.

The complex structure of the cell and its nontrivial diffractive properties make it difficult to perform precise force measurements with optical tweezers within living cells [14, 23]. Also, the lack of knowledge of the size and refractive index of the trapped particle renders most methods inadequate [24]. For instance, as the Brownian motion of a particle in such a viscoelastic environment is different from that within a viscous environment [25–27], the power spectrum analysis is not directly applicable inside a living cell.

One proposed way to retrieve the optical force acting on a trapped particle within a cell is by detecting light momentum changes [28–31]. However, using this method, the spring constant characterizing the strength of the optical trap, the position of the particle and the viscoelastic properties of the cytoplasm cannot be deduced. It has also been suggested to calibrate optical tweezers within a cell with resort to a model for the viscoelastic response of the cell's cytoplasm. This procedure thus relies on specific assumptions about the cytoplasm. It is described in ref. [32] and in the subsequent chapter of this book.

The active–passive calibration procedure presented here is based on the fluctuation-dissipation theorem (FDT) and the only assumption regarding the cytoplasm is that it can be treated as a viscoelastic medium. The calibration procedure assumes that the response of a system in equilibrium to small externally driven perturbations is the same as its response to internal fluctuations. In other words, the procedure is based on the assumption that the amplitude of the driving motion is at the order of magnitude of the Brownian motion occurring in the equilibrium state. For calibration purposes, perturbations can be caused by oscillating the sample with respect to the trapping laser, either by moving the sample stage or by oscillating the trapping laser itself [33–35]. A more detailed theoretical background can be found in refs. [36–38].

This calibration method was proposed in ref. [38] and demonstrated in actin networks and yeast cells in refs. [36, 37]. The method can be applied to any viscoelastic medium without any prior knowledge or assumptions about the medium's viscoelasticity and with no need for external calibration [39, 40]. In addition, no prior knowledge of the shape and size of the trapped particle is necessary. The combination of active and passive measurements for quantitative in vivo measurements has been proposed and applied in refs. [6, 34, 38, 41–44]. By combining active and passive measurements, the absolute value of the trap's spring constant for every trapped object in the cell's cytoplasm can be determined. Additionally, the viscoelastic properties of the medium can be inferred from this calibration procedure, as it also allows quantifying the viscoelastic moduli.

2 Materials

2.1 Experimental Setup

1. Infrared laser for trapping, here: 1064 nm Nd:YVO_4 laser (5 W, Spectra Physics BL-106C).
2. Optical microscope with high NA objective, here: Leica DMIRBE with Leica HCX PL APO 100×, NA = 1.4, OIL CS.
3. Quadrant photodiode (QPD), here: S5981, Hamamatsu.
4. CCD camera, here: A11 KODAK Pike, 60 Hz.
5. Piezo-stage for stage-oscillation, here: Physik Instrumente P-517.3CL.
6. PC with rapid data acquisition card, here: NI PCI-6040E.

2.2 Cell Sample

Any type of live cells with naturally occurring organelles, like lipid granules, that may be trapped by an optical trap due to a higher refractive index of the organelle than of the surrounding cytoplasm. In the case described here, SPK10 wild type *S. pombe* cells were used.

2.3 Cell Growth

1. YPD broth: Common liquid growth medium for yeast culture. If purchased in powder form, follow instructions to dissolve in water.
2. AA medium: Medium containing 1.7 g Bacto yeast nitrogen base without amino acids or ammonium sulfate, 5 g ammonium sulfate, 2 g drop-out mix, 450 ml H_2O. Autoclave before adding 50 ml 40 % glucose. Drop-out mix: 0.4 g para-amino benzoic acid, 4 g L-leucine, 2 g each of needed amino acids (L-alanine, L-arginine, L-asparagine, L-cysteine, L-glutamine, L-glutamic acid, L-glycine, L-histidine, L-isoleucine, L-lysine, L-methionine, L-phenylalanine, L-proline, L-serine, L-threonine, L-tryptophan, L-tyrosine, L-valine, myo-inositol, adenine, uracil).

3. AA minus leucine agar plates: Add 20 g Bacto agar in 500 ml H_2O to AA medium not containing L-leucine and pour into plates.

2.4 Sample Chamber

1. Sterile and clean slides (25 × 60 mm, thickness 1 mm) and coverslips (18 × 18 mm, thickness 0.17 mm).
2. 100 % ethanol.
3. millipore H_2O.
4. Poly-L-lysine: Use high molecular weight (MW) poly-L-lysine (>300 kDa), as high MW molecules have more attachment sites.
5. Vacuum grease.
6. Double-sided scotch tape: optional.
7. Mechanical tweezers.
8. Syringe.
9. Petri dish.

3 Methods

3.1 Optical Tweezers Setup

The presented calibration procedure can be utilized by a great variety of optical tweezers setups. It is, however, necessary to be able to make fast and precise position measurements, which are most conveniently done by a photodiode, and to oscillate either the laser or the sample stage. In the experiments from which data are shown in this chapter, the optical tweezers setup was implemented by directing the infrared laser into an inverted microscope (Fig. 1); further details for this particular setup can be found in ref. [45]. Briefly, the laser is focused into a diffraction-limited spot onto the sample plane through an oil immersion objective. After passing through the sample, the laser light is captured by a condenser and projected onto a QPD placed conjugate to the condenser's back-focal plane, allowing for high-precision positional detection [46, 47]. A CCD camera, mounted on the side port of the microscope, establishes a second, bright-field based detection system to record movements of sufficiently optically dense objects in the sample plane (Fig. 1).

The sample is mounted on a piezo-electric translation stage, which can oscillate the sample. The voltage signals providing the positions of the stage and the voltage signals of the QPD, generated by the light scattered by a trapped particle, are read out simultaneously by an acquisition card (*see* **Note 1**). Alternatively, the particle of interest can be oscillated by using an acousto-optic deflector (AOD) instead of a Piezo-stage [34]. This can be accomplished by placing an AOD in the beam path before the laser enters the microscope at a plane conjugate telecentric to the back-focal plan of the microscope objective (Fig. 1) (*see* **Notes 2** and **3**).

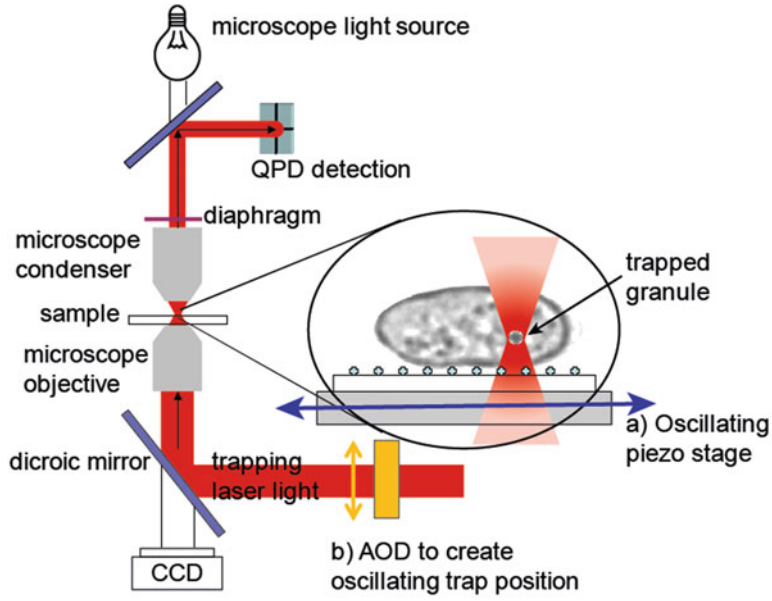

Fig. 1 Experimental setup: a 1064 nm laser is focused through an oil immersion objective into a microscope to form the optical tweezers. The movement of a lipid granule inside a living *S. pombe* cell is recorded by a QPD placed conjugate to the back-focal plane of the condenser or by the use of a CCD camera. The sample is mounted on a piezo stage, which is used to position the cell of interest in the focus and to oscillate the sample in a controlled fashion. Alternatively, the trapped granule can be oscillated with respect to the sample chamber by placing an AOD in the beam path before the laser enters the objective lens

3.2 Cell Sample Preparation

1. Culture SPK10 wild type *S. pombe* cells on AA minus leucine agar plates at 30° for 18–20 h and store them afterwards at 4 °C.
2. The day before the cells are needed for experiments, transfer a fraction of the cells from the plates to liquid YPD medium and grow them in a shaking bath overnight at 30°.
3. Centrifuge cells for 5 min at 1764 × *g* (5000 rpm). (i.e. 0.35 g per rpm).
4. Remove the supernatant.
5. Resuspend cells in AA medium with a dilution factor of 10–100. Use AA medium instead of the YPD medium during experiments, as the YPD medium interferes with the poly-L-lysine coating.

3.3 Perfusion Chamber

1. Dissolve poly-L-lysine in millipore H_2O (to a final concentration of 1 mg/ml).
2. Place a clean and sterile coverslip with mechanical tweezers into a petri dish and add 50 µl of poly-L-lysine solution on top. Poly-L-lysine promotes the adhesion of the cells to the glass surface

by enhancing electrostatic interaction between its positively charged sites and the negatively charged ions of the cell membrane.

3. Rock coverslips for 30 min at room temperature.
4. Wash coverslip at least ten times with millipore H_2O to remove any free polyamino acids, which can be cytotoxic.
5. Rinse a slide with absolute ethanol and let dry. Tip: Lean slide on the side of the petri dish to dry.
6. Fill syringe with vacuum grease.
7. When the slide is dry, apply two thin lines of vacuum grease or two lines of two layers of double-sided scotch tape, to create a sufficiently high chamber, in parallel along the long sides of the slide (Fig. 2).
8. Place the poly-L-lysine coated coverslip (from **step 4**) on top of the scotch tape/vacuum grease (poly-L-lysine side towards the slide).
9. Perfuse a suspension containing living cells into the assembled sample chamber.
10. Seal the open ends of the chamber with vacuum grease.

When working with different cell types, cells may adhere well to the coverslip without the use of poly-L-lysine or by using alternative adhesion-promoting reagents such as gelatin or collagen [48]. In this case, leave out **steps 1–4** and use normal growth medium in **step 9** to fill the chamber. Of course, cells can also be seeded in more complex microfluidic environments allowing for a constant flow across the cells, for buffer exchange or for perfusion with fresh media.

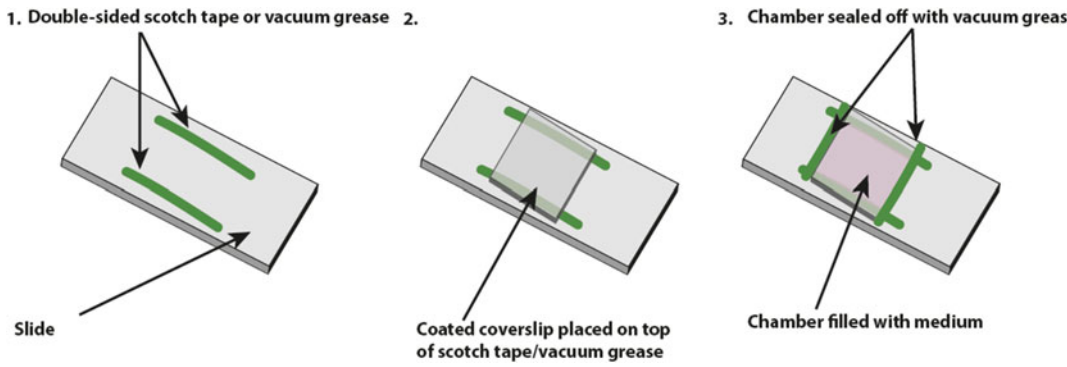

Fig. 2 Preparation of a sample chamber: (1) Apply double-sided scotch tape or vacuum grease to the sides of a clean slide. (2) Place a coated coverslip on top of the scotch tape/vacuum grease, with the coated side facing towards the slide. (3) Fill chamber with cells or beads in medium and seal the open ends with vacuum grease

3.4 Introduction to the Active–Passive Calibration Procedure

The main part of this chapter describes the active–passive calibration procedure. In the following sections, we outline the protocols for the passive (Subheading 3.5) and active calibration measurements (Subheading 3.6).

Assuming that a particle trapped in an optical tweezers setup experiences a harmonic potential, the force, F, acting on the particle can be determined as: $F = \kappa x$, with x being the displacement of the particle from the equilibrium position and κ being the spring constant, which characterizes the trapping stiffness (*see* **Note 4**). By measuring x and the spring constant κ, the force can be extracted. Hence, in order to perform absolute force measurements inside a living cell or organism, it is crucial to accurately determine κ. In the following, we will demonstrate how the active–passive calibration method can be used to extract an absolute value for κ, which, in connection with a measurement of the particle's position, x, is all that is needed to quantify the force of a trapped particle within a living cell. Additionally, this method allows for quantification of the cell cytoplasm's viscoelastic properties through extraction of the viscoelastic moduli, G' and G''.

3.5 Passive Calibration Measurements

For the passive measurements, the optical trap is focused onto a particle and the position of the particle, $x_p(t)$, is recorded by the QPD (Fig. 3). The thereby acquired time series is used to calculate the power spectrum $P(\omega)$ of the positional fluctuations within the trap (Fig. 3):

$$P(\omega) = \lim_{T_{\text{Meas}} \to \infty} \frac{|\widetilde{x}_P(\omega)|^2}{T_{\text{Meas}}}. \tag{1}$$

Here, $\widetilde{x}_P(\omega)$ is the Fourier transformed position of the particle in the trap, T_{Meas}, the duration of the measurement and $\omega = 2\pi f$ is the angular frequency with f being the normal frequency.

Steps for extracting the power spectrum:

1. Place sample on the sample stage, so that the coverslip faces the objective.
2. Adjust condenser height: Set up Köhler illumination for optimal contrast and precision.
3. Find laser in the sample plane and adjust the QPD position, so that the laser hits the center of the photodiode.
4. Adjust data amplification if necessary.
5. Choose a granule for data acquisition; record and store an image for later use (see example in Subheading 3.8).
6. Record the position, $x_p(t)$, of the trapped granule for 3 s with the QPD at a sampling rate of 22 kHz [58].

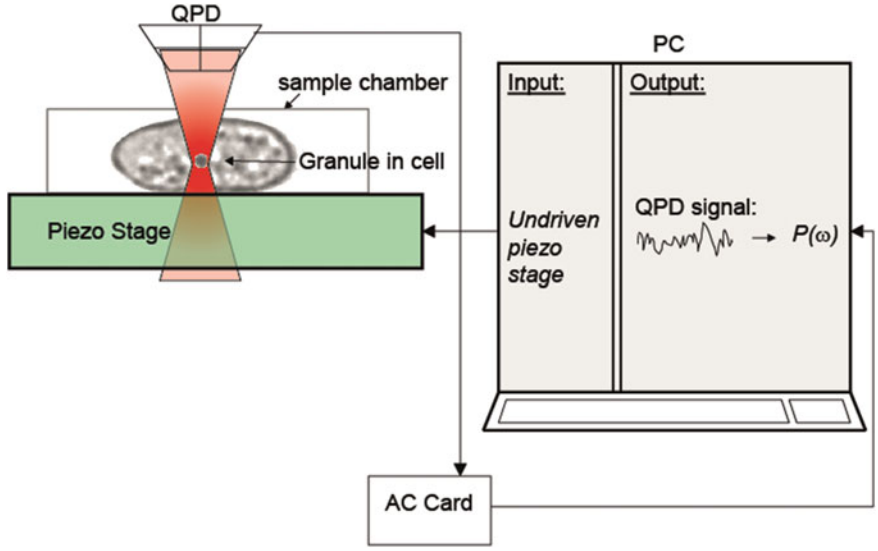

Fig. 3 Illustration of the passive measurement: A power spectrum, $P(\omega)$, is obtained by tracking and recording the position of a lipid granule inside a living *S. pombe* cell using a fixed optical trap and a fixed stage

7. Repeat this measurement 30 times.
8. Calculate an average power spectrum $|P(\omega)|$ from the 30 measurements [36].

3.6 Active Calibration Measurements

To calibrate an optical trap in a viscoelastic environment, not only the information from the passive measurements, but also information on how the particle moves in such a viscoelastic environment is needed. To obtain this additional information, the trapped particle is moved by oscillating the sample stage with respect to the trapping laser. The movement causes a small perturbation of the system. Using linear response theory, the linear response function of the medium, $\chi(\omega)$, relates the Fourier-transformed external force, $\widetilde{F}_{\text{ext}}(\omega)$, to the average Fourier-transformed position of the particle, $\langle\widetilde{x}(\omega)\rangle$:

$$\langle\widetilde{x}(\omega)\rangle = \chi(\omega)\widetilde{F}_{\text{ext}}(\omega). \tag{2}$$

The linear response function, $\chi(\omega)$, can therefore be regarded as an inverse spring constant.

In order to retrieve an absolute value for the spring constant, κ, and the viscoelastic modulus, $G(\omega)$, it is necessary to convert the measured quantities to SI units. Additionally, it is necessary to quantify the error in the system due to time delay between the electronic systems that record the position of the stage and the position of the trapped particle. To accomplish this, three steps are added to the calibration procedure: A direct positional calibration, a pixel calibration and a phase correction calibration, which are outlined below.

3.6.1 Active Force Calibration

During the active force calibration, the trapped particle is moved sinusoidally by oscillating the sample stage. This step is illustrated in Fig. 4. The position of the stage is recorded and given by $x_S(t) = A_S \sin(\omega t + \phi_S)$, with A_S being the amplitude, ϕ_S the phase, and ω the driving frequency of the stage movement. At the same time, the position of the driven particle is recorded by the QPD and given as, $x_P^{(dr)}(t) = A_P \sin(\omega t + \phi_P)$ with A_P and ϕ_P the amplitude and phase of the trapped and driven particle. The Fourier-transformed positional information of the trapped particle and the stage are used to calculate the relaxation spectrum, defined as

$$\widetilde{R}(\omega) = \frac{\widetilde{x}_P^{(dr)}(\omega)}{i\omega\widetilde{x}_S} = \frac{A_P}{\omega A_S}(\sin\Delta\phi - i\cos\Delta\phi). \tag{3}$$

The relaxation spectrum can therefore be extracted through the phase difference, $\Delta\phi$. The phase difference is given by:

$$\Delta\phi = \phi_P - \phi_S. \tag{4}$$

Steps to extract amplitude and phase of the sinusoidal movement:

9. With the same granule as in the previous passive measurement (repeat **steps 2–4** if needed), drive system sinusoidally with a set amplitude. Choose the amplitude carefully (*see* **Notes 4–6**).

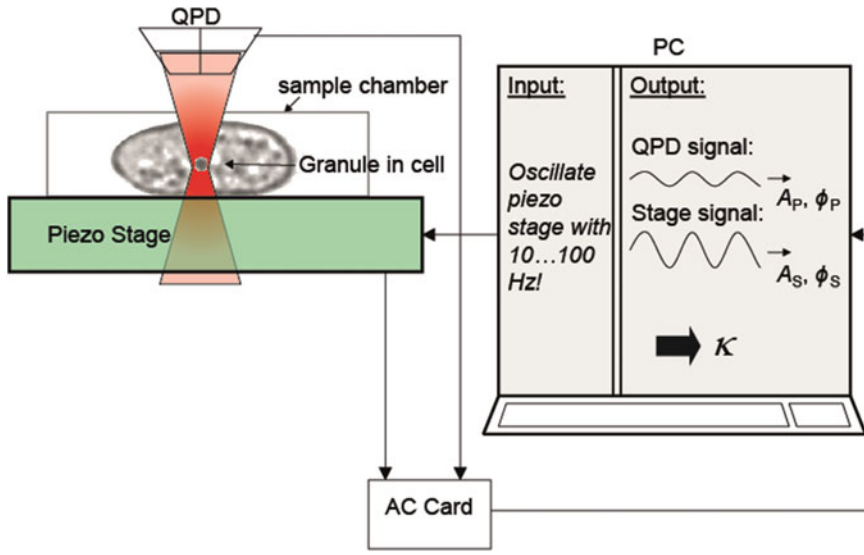

Fig. 4 Illustration of the active force measurement. Here, the trapped particle is a lipid granule inside a cell that is moved sinusoidally by oscillating the piezo stage. The movement of the stage is recorded using a position feedback signal output from the piezo stage, and the movement of the granule is measured by the QPD. The output data is fit to the relaxation spectrum to extract the amplitude of the particle movement, A_P, and the phase difference, $\Delta\phi$

$A_S = 100$ nm was used to obtain the data presented in Subheading 3.8 *Example of Experimental Data*.

10. Change frequency of the sinusoidal movement in 5 Hz decrements. The frequency has to be chosen appropriately, as it can otherwise render the FDT invalid (*see* **Note 3**). It is also advised to avoid frequencies corresponding to excessive instrumental noise (*see* **Note 7**).
11. Record the granule position with the QPD for 10 s at a sampling rate of 10 kHz [36].
12. Record sinusoidal movement of the piezo stage.
13. Check the set amplitude, A_S, by fitting the recorded positions. The amplitude and the oscillation frequency of the stage movement are in principle already known, as they are set during the experiment. Nevertheless, there might be differences between set values of the amplitude and actual motion, due to nonuniform piezo response vs. frequency (*see* **Note 2**).
14. Extract the amplitude of the trapped particle, A_P, and the phase difference, $\Delta\phi$, by fitting the relaxation spectrum given in Eq. 3 to the experimental data. Consistency checks are recommended (*see* **Note 8**).
15. Take an image of the trapped granule, to allow for an additional consistency check; see example in Subheading 3.8. For yet another consistency check, redo the passive measurement, **steps 6–8**.

3.6.2 Direct Positional Calibration

The direct positional calibration is an additional measurement that is needed to determine the conversion factor β, it is illustrated in Fig. 5. β translates the voltage output of the QPD, x_V (given in Volts), to SI units, x_{SI} (in meters), and is defined as the ratio

$$\beta = \frac{x_{SI}}{x_V}. \tag{5}$$

Steps to extract β:

16. Follow **steps 1–4** from the passive measurement.
17. Drive stage for 10 s at a frequency of 2 Hz and record the movement of the trapped particle separately with the CCD camera and with the QPD. We conduct these two measurements subsequently but with identical conditions because we close the diaphragm of the condenser to increase the image contrast when recording with a CCD camera, while we leave the diaphragm open when acquiring with the QPD [49].
18. Use sampling rates of 10 kHz for the QPD and 60 Hz for the CCD camera and repeat the oscillation cycles 20 times per amplitude.

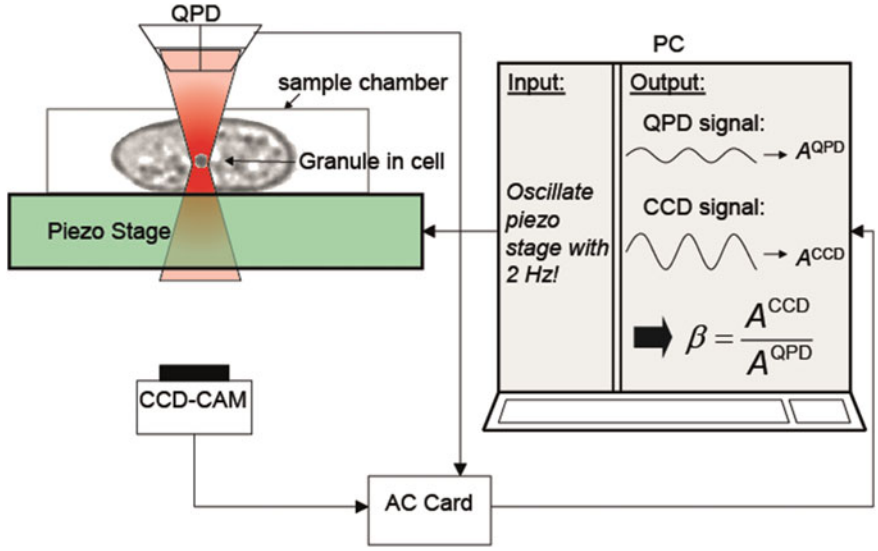

Fig. 5 Direct positional measurement to convert the QPD voltage output to SI units. The stage is driven sinusoidally and the position of the trapped particle is recorded with both a QPD and a CCD camera. Fits of the QPD and CCD signals to sinusoidal functions are then used to extract the amplitudes to obtain the conversion factor β

19. Fit the obtained data with a sinusoidal fit to extract the amplitudes from the two signals.
20. Calculate the conversion factor, β, using the extracted amplitudes.

It is advisable to check that β is independent of the driving amplitude as illustrated by Fig. S2 in the supplementary data of reference [36].

3.6.3 Pixel Size Calibration

In order to correctly determine the conversion factor, β, the effective pixel size, α, of the camera needs to be known (in nm per pixel). This step is illustrated by Fig. 6.

Perform the following steps to extract α:

21. Take 50 μl of a bead solution and add 950 μl millipore H_2O (or a different buffer such as PBS). Mix by pipetting up and down.
22. Place bead solution into a centrifuge and spin for 15 min at 1764 × *g* (5000 rpm) (i.e. 0.35 g per rpm).
23. Resuspend in water or buffer at the desired dilution. Keep stock solution in refrigerator and vortex before use to break up aggregates.
24. Prepare sample chamber as described in Subheading 3.3, but fill the chamber with the prepared polystyrene bead solution instead of cell solution.

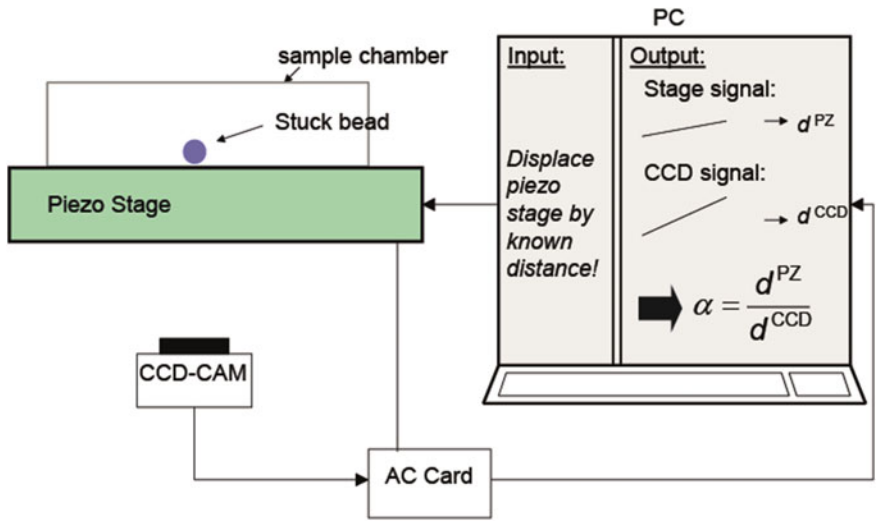

Fig. 6 The pixel size is determined by moving a stuck bead in discrete steps in axial and lateral directions while images are continuously acquired by the CCD camera. Binary mapping is used to extract the positional change in lateral and axial directions from the images and to calculate the conversion factor α

25. Find a bead stuck to the bottom of the sample chamber.
26. Move the stage in predefined steps, d^{PZ}, in lateral and axial directions, while imaging simultaneously with the CCD camera.
27. Use Matlab or any software available in your lab (e.g., ImageJ) to transform the bead in the images into a bright ring on a black background using binary mapping.
28. Use your preferred software to determine the position of the center and the diameter of the ring for each image. The position of the center of the ring is interpreted as the lateral position and the diameter as the axial position of the bead. To determine the lateral position, track the position of the center of the ring by counting the number of pixels the center moved. Richardson et al. [50] found that the diameter of the ring is linearly related to the axial position with respect to the focus of the objective. The diameter of the ring can be determined by fitting a box around the ring. A custom-written program was used to extract the lateral and axial position of the bead presented in Subheading 3.8 *Example of Experimental Data*.
29. Plot lateral/axial position (given in pixels) as a function of the stage displacements (given in nm).
30. Extract the effective pixel size α from the plot by using a linear fit.

Alternatively, freely available software such as "Video Spot Tracker" has also proven useful for tracking beads and trapped intracellular granules.

In our setup, the 100× objective together with the additional magnifying optics gives an effective pixel size of $\alpha = (5.56 \pm 0.02)$ nm/pix for the CCD. Further information can be found in ref. [50].

3.6.4 Phase Correction Calibration

The voltage output of the QPD and the positional information of the piezo stage are acquired by an acquisition card. The various channels of the acquisition card allow for simultaneous read out of this data. However, when reading out channels simultaneously there is a time delay between the recording of the individual channels, which can cause systematic errors and which therefore needs to be taken into account (*see* **Note 1**).

As the acquisition of the bead position is delayed compared to the stage position by a delay time $t^{(\mathrm{del})}$, the phase difference in Eq. (4) needs to be corrected for this delay

$$\Delta\phi^{(\mathrm{corr})} = \Delta\phi^{(\mathrm{fit})} - \Delta\phi^{(\mathrm{del})}. \tag{6}$$

$\Delta\phi^{(\mathrm{fit})}$ is found as described in Subheading 3.6.1, **steps 9, 12–14** by fitting a sinusoidal function to the information obtained from the QPD and the stage position of the trapped particle, the procedure is illustrated in Fig. 7.

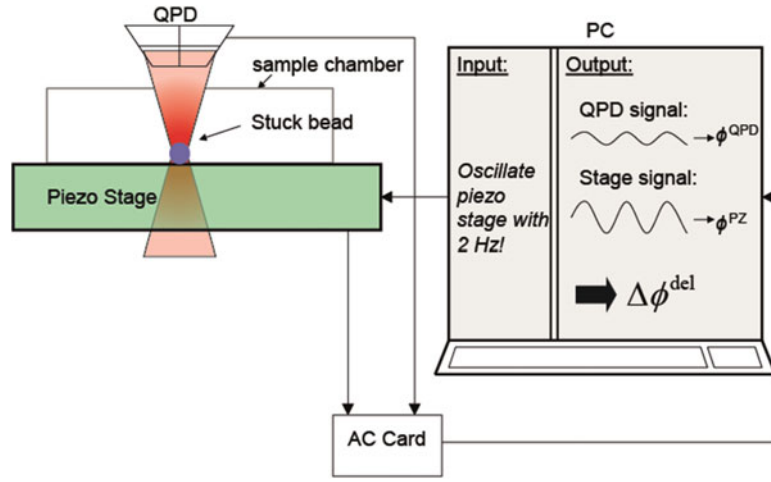

Fig. 7 Phase correction calibration to determine the time delay between acquisition card channels. The position of a stuck bead is recorded by the QPD, while the stage is oscillated sinusoidally with 2 Hz. The phase difference between the sinusoidal fits to the QPD and stage signals gives the time delay between the channels

Steps to determine the time delay between the channels of the AC card:

31. Prepare a sample chamber with beads stuck to the bottom coverslip as in **steps 24** and **25**.
32. Follow **steps 1–4** from the passive calibration measurement.
33. Find a bead and oscillate sample sinusoidally at a frequency of 2 Hz.
34. Record the movement of the bead with the QPD and the stage position.
35. Fit both signals with a sine-wave function (since the bead is stuck to the coverslip it should move exactly like the stage).
36. Calculate the phase difference of the sinusoidal fits to the stage and QPD signals. This phase difference reveals the time lag due to the acquisition process.

This phase correction calibration procedure only needs to be performed once for a given acquisition card and is in our case determined to be (467 ± 65) μs for the acquisition card used here [37] (*see* **Note 1**).

Steps 21–36 need only be completed once, whereas **steps 1–15** can be carried out for several granuli within the same cell, providing in particular information about variations in the viscoelastic properties of the cytoskeleton at different locations within the cell. **Steps 16–20** are preferably repeated for each new sample.

3.7 Active–Passive Calibration to Extract Spring Constant and Viscoelastic Moduli

Using the information gained from the active and passive calibration procedures, the spring constant can be found using this equation:

$$\kappa - \omega^2 m = 2k_B T \frac{Re\left(\widetilde{R}(\omega)\right)}{P(\omega_S)} = \frac{2k_B T}{P(\omega_S)} \frac{A_P}{\omega_S} \sin(\Delta\phi). \qquad (7)$$

Perform the following steps to determine κ and the viscoelastic moduli using Eq. 7:

1. The spring constant as function of the stage oscillation frequency, ω_S, is calculated by inserting the parameters A_P, $\Delta\phi$, $P(\omega_S)$ and ω_S into Eq. 7. Here m stands for the mass of the trapped particle. However, it is not necessary to know the mass of the trapped particle because the frequency ω is so small that the term $\omega^2 m$ can be neglected, as it is significantly smaller than the other terms in the equation.
2. Based on the obtained value for $\kappa(\omega)$, the elastic modulus $G(\omega)$ can be found. This modulus consists of a real part, which characterizes the elastic response, and an imaginary part characterizing the viscous response of the medium. The real part is

also known as the shear storage modulus G' and the imaginary part is the shear loss modulus G''.

$$G(\omega) = \frac{i\omega}{6\pi r}\left(\kappa - \omega^2 m\right) \frac{\widetilde{R}(\omega)}{1 - i\omega\widetilde{R}(\omega)}. \tag{8}$$

3. Calculate the elastic modulus $G(\omega)$ by inserting the values for $\kappa(\omega)$ and for the relaxation spectrum $\widetilde{R}(\omega)$, defined in Eq. 3. The radius of the trapped particle is denoted as r and can be extracted from the bright field images. The average radius of the granules used herein was determined to be (0.6 ± 0.1) μm [36].
4. The spring constant can be used to determine the linear response function (Eq. 2) of the medium:

$$\chi(\omega) = \frac{1 - i\omega\widetilde{R}(\omega)}{\kappa - \omega^2 m} \simeq \frac{1 - i\omega\widetilde{R}(\omega)}{\kappa}. \tag{9}$$

5. The effective spring constant, which is the spring constant that combines all elastic forces from the optical trap and from the viscoelastic medium acting on the trapped particle, is given as the inverse linear response function:

$$\kappa_{\text{eff}} = \frac{1}{|\chi(\omega)|}. \tag{10}$$

3.8 Example of Experimental Data

This section gives an example of an experimental data set, where lipid granules within living *S. pombe* cells were used as probes for the calibration of the optical trap. Data were acquired by focusing the trapping laser onto a chosen lipid granule and time series of the positions visited by the granule were recorded. Bright field images showing the cell and the cytoplasmic granules were acquired before and after trapping a granule, to visually ensure that other granules or organelles had not entered the trap during data acquisition (Fig. 8). A time series was disregarded, if additional objects were found or if the trapped granule changed shape.

The spring constant κ and the viscoelastic moduli G' and G'' were determined using the described active–passive calibration procedure.

The spring constant of the optical trap was calculated using Eq. 7. The viscoelastic environment within the cells can also contribute to the total effective spring constant, which describes the total elastic force acting on a lipid granule. The effective spring constant, κ_{eff}, which takes into account the viscoelastic environment, was determined using the linear response function, $\chi(\omega)$ (Eq. 9), and is simply calculated from the absolute value of the linear response function (Eq. 10). Figure 9a shows κ and κ_{eff} as a function of driving frequency. The depicted asterisk in Fig. 9 is the value $k_B T/\langle x_P{}^2\rangle$, which would be the value of the trap's spring constant in a purely viscous system. In a viscoelastic environment,

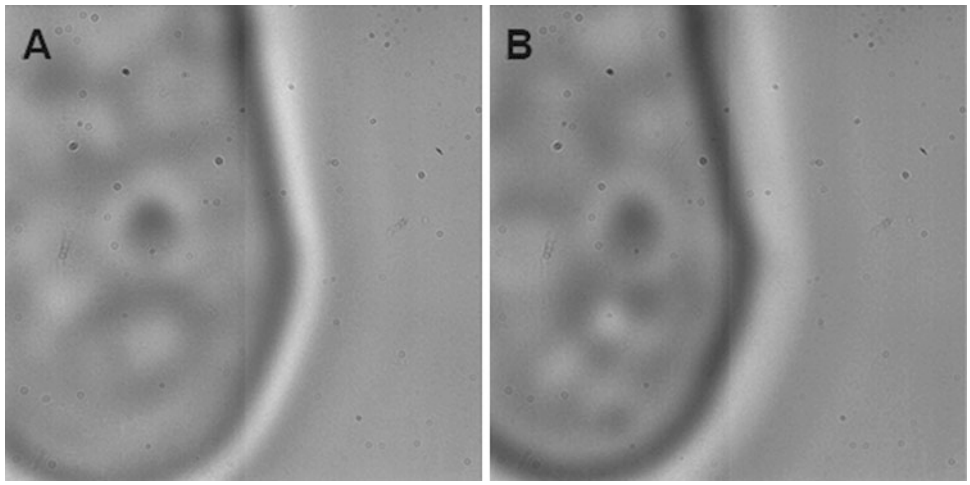

Fig. 8 Images of a lipid granule in an *S. pombe* cell, (**a**) before and (**b**) after the calibration procedure, indicating that neither the size nor the number of trapped granules have changed

however, this value can be understood as an independent measure of a low-frequency effective spring constant. This interpretation is in agreement with the values of $k_B T/\langle x_P{}^2 \rangle$ and the effective spring constant given in Fig. 9.

The viscoelastic moduli of the cells' cytoplasm were obtained from Eq. 8 using the measured average radius of the lipid granule, r (0.6 ± 0.1 μm, *see* Subheading 3.5). Figure 9b displays the real part G', the storage loss modulus, describing the elastic response of the system. The imaginary part G'' corresponds to the viscous response of the viscoelastic modulus. Both parts are functions of the driving frequency. For example, Fig. 9b shows that the storage loss modulus increases for driving frequencies below ~40 Hz, while it becomes largely insensitive to driving frequencies in the range of ~40 Hz and ~70 Hz. The observation of a plateau in the frequency response of the storage loss modulus is typical for a semi-dilute polymer solution [27].

4 Notes

1. *The acquisition card has to be chosen carefully:* Several steps of the active–passive calibration procedure require the simultaneous recording of stage and particle position. However, reading out this information from different channels simultaneously comes with a time delay. This time delay introduces systematic errors to the experimental results and should therefore be taken into account. The delay time for the acquisition card used is (467 ± 65) μs [36, 37]. When purchasing an acquisition card, it is therefore imperative to choose the card carefully to ensure fast readout of different channels.

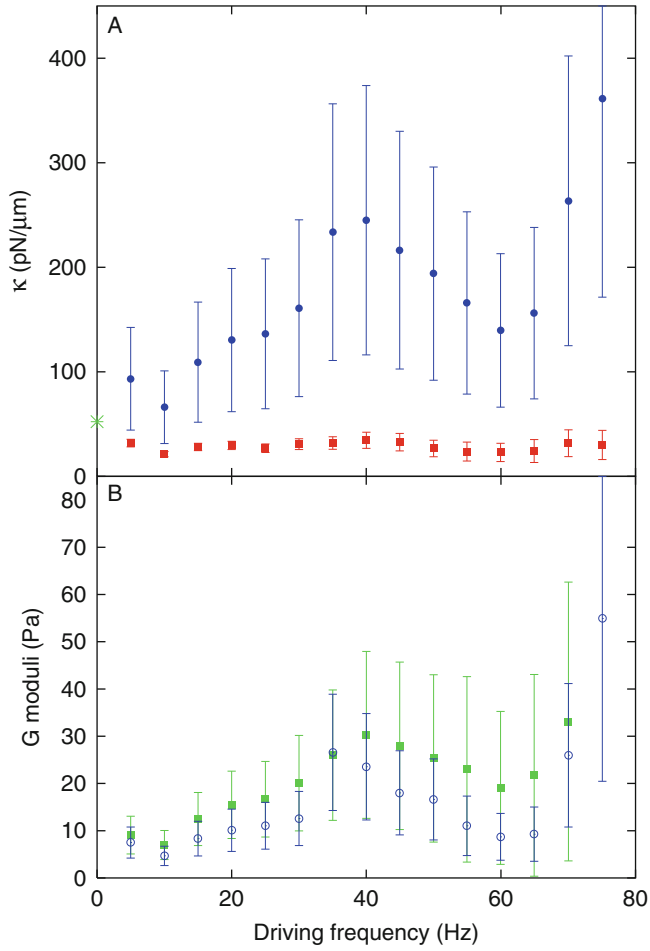

Fig. 9 Spring constant and viscoelastic moduli as a function of driving frequency. (**a**) Spring constant, κ, characterizing the optical trap and (**b**) viscoelastic moduli of one lipid granule as a function of the driving frequency (5–75 Hz). (**a**) The graph depicts the effective spring constant, κ_{eff} (*blue filled circles* with *error-bars*), which includes contributions from the trap and the viscoelastic local environment, and the spring constant κ (*red filled squares* with *error-bars*), which solely characterizes the trap. The *green asterisk* on the ordinate axis corresponds to the value of $k_B T/x_P^2$. (**b**) Real part (storage; *blue open circles*) and imaginary part (loss; *green filled squares*) of the viscoelastic modulus G as function of driving frequency. The error bars in (**a**) and (**b**) were calculated using error propagation of systematic instrumental uncertainties and statistical errors

2. *Stage or laser driving, what to choose?* Oscillating the trapped particle with either a stage or the laser beam using an AOD has both advantages and disadvantages. Starting from a technical perspective, stage driving is easier to implement and instrumental efforts are less demanding in comparison to laser driving. However, the bandwidth of available frequencies is limited. State-of-the-art stages are capable of oscillations with frequencies in the order of hundreds of Hz [37]. We also observed that the stage in our setup does not reach the set amplitude at higher oscillation frequencies, which is a problem that should be taken into account [36]. AOD-based laser beam

oscillations on the other hand, can be driven with significantly higher frequencies (see subsequent chapter) and therefore with frequencies well above those at which active biological processes and noise occur [34] (*see* **Note 3**). Additionally, the use of laser driving omits the need of a separate calibration procedure to obtain the conversion factor β to convert from voltage to metric units, which is prone to large errors. The conversion factor can be obtained directly by the ratio between the set oscillation amplitude of the laser and the voltage output of the QPD. When using laser driving, one should still be aware and acknowledge the limitations of this method, see for example refs. [33, 35]. Finally, it is important to choose an oscillation amplitude that does not exceed the harmonic trapping region of the trap [50] and one that still ensures that the perturbations are small.

3. *Choose the best oscillating frequencies:* The active–passive calibration procedure is based on linear response theory. The perturbation caused by the active movement in the calibration procedure should therefore be small to ensure a linear response of the system. In living cells, however, active processes take place and these processes can render the fluctuation dissipation theorem (FDT) method invalid in certain frequency ranges. For example, it has been shown that the fluctuations of beads in an actin network with active molecular motors or in MLO-Y_4 cells violate the FDT at frequencies below 10 Hz [51, 52], implying that the system is governed by nonequilibrium processes at lower frequencies. Using only higher frequencies can help avoiding recordings in this problematic frequency range. The use of an AOD, which can operate even in the kHz range, may therefore be preferable over stage driving which is difficult to do in the kHz regime. It is worth noting, however, that the active biological processes should reveal themselves in the calibration process, as the extracted spring constant κ would in this case not be independent of driving frequency. We have found [36] that in our experiments κ does not change with the driving frequency, which validates the use of the linear response theory for the frequency range used (5–75 Hz). However, in our experiments, κ exhibited relatively large variations from one cell to another and at different locations within a cell. These variations are likely caused by differences in the local cellular cytoskeleton and/or differences in the size, shape and refractive index of the trapped lipid granules. Considering that these parameters will vary from one trapped particle to the next, calibration of the trap for each trapped object is necessary, especially for precise force measurements [36].
4. *Choose the best oscillation amplitude:* Larger oscillation amplitudes lead to larger deflections of the trapped particle and therefore to a better signal to noise ratio. However, the

amplitude cannot be chosen arbitrarily large, as there are constraints on the size of the amplitude. First, the trapped particle needs to stay within the linear detection region of the QPD [53]. Secondly, the trapped particle needs to stay within the harmonic trapping potential of the optical tweezers [50]. Thirdly, there are constraints given by linear response theory on which our calibration procedure is built. For the linear response theory to be upheld, the oscillatory motion must only generate a small perturbation of the equilibrium system (*see* **Note 3**). For this reason, only small amplitudes can be used [38]. Taking these conditions into account, the driving amplitude should be chosen in a way such that the amplitude of the trapped particle is roughly equal to the half width of the trap, $(k_B T/\kappa)^{1/2}$. In doing so, a linear response of the system will be ensured [37].

5. *Determine the QPD's linear regime:* The voltage output of the QPD is proportional to the distance a particle moves in the optical trap within a certain interval, which is referred to as the linear region. When executing the active–passive calibration procedure it is important that the active oscillations of the sample do not exceed this linear region of the QPD (*see* **Note 4**). The linear region of the QPD can be defined by moving a stuck bead through the laser focus with constant velocity. From the obtained data, the regime with a monotonic linear voltage response can be determined [36]. When staying within this linear region of the QPD, it is not necessary to obtain the conversion factor β to retrieve the force. Because the position measured by the QPD is given in Volts, the amplitude of the stage-driven particle motion, A_P, and the power spectrum, $P(\omega_S)$, are given in V and $V^2\ s^{-1}$, respectively. If the spring constant κ is determined from these parameters, then the units of κ are given as $N\ V^{-1}$. The resulting force is then given in SI units, since the position of the trapped particle given in Volts times the spring constant gives Newtons, N. However, if absolute values for κ and $G(\omega)$ are needed, determination of β is required [36]. In micro-rheological measurements, one needs only information about the characteristic power law for the viscoelastic moduli of the cell cytoplasm, $G'(\omega)$, $G''(\omega) \propto \omega^{\delta}$. Information about the value of δ can for example be obtained using optical tweezers without the knowledge of an absolute trap spring constant because δ is also reflected in the mean squared displacement calculated from the positions visited by a particle [25, 48]. These types of measurements have brought insight into the diffusion of tracer particles [25, 48, 54, 55] and the viscoelastic moduli of the cytoplasm [56, 57] and of reconstituted polymer networks [40, 41].

6. *Choose the right QPD and CCD axis:* Particle trajectories normally follow the direction of the sinusoidal perturbation (laser driven or stage driven). It is convenient to have both QPD and CCD detectors positioned with one of their lateral axes parallel to the stage/laser driving direction, which reduces the calibration to a unidimensional problem. Otherwise bidimensional trajectories would need to be projected onto the active perturbation axis before sinusoidal fitting, and care should be taken in having the appropriate β calibrations for all axes. Moreover, once the axes are aligned, the directions of movement might be parallel or antiparallel, depending on the orientation of the stage/QPD. Note that the measurement of the conversion factor β (described in Subheading 3.6.2, **steps 16–20**), which is given by the ratio of amplitudes, yields an absolute value. The sign of β depends on every system and should be determined once. To determine the sign, move a stuck bead with the stage away from the trap center along the axis of interest and measure the change of the sign of the QPD signal after displacement. If the stage and QPD signals change in opposite directions, the sign of β should be set negative for the system, to ensure that a zero phase delay in the stage-particle sinusoidal signals corresponds to the particle and the stage moving together in the same direction.
7. *Avoid vibrations:* Vibrations in the microscope setup might arise at specific frequencies, depending on mechanical resonances of the system, and will show up as peaks in the passive power spectrum. Active–passive measurements should be avoided in the region of noise peaks, since they might mask the actual particle oscillation, and affect the measurement of the phase difference between particle and stage.
8. *Do consistency checks:* The full calibration procedure with stage driving takes about 5 min to complete, and the cellular activity does not stop. The trapped granule might interact with other elements in the cell cytoplasm during this time, and undergo unexpected movements that can affect the measurement of the trap stiffness. Hence, to make sure the experiment was not affected by unexpected movements, it is recommended to confirm the following observations: (1) no significant motion occurs perpendicular to the driving direction, (2) the mean position does not change, both during active and passive measurements, (3) the granule does not drift axially during the experiment, and (4) the particle vs. stage plot is elliptical (superposition of two sinusoidal signals with a relative phase). Deviations from the ideal elliptical behavior might indicate the presence of other organelles in close vicinity of the trapped granule, or possibly that the granule moved out of the linear region (e.g., if driving amplitude is too large). An example of such a consistency check is illustrated in Fig. 10, where panel

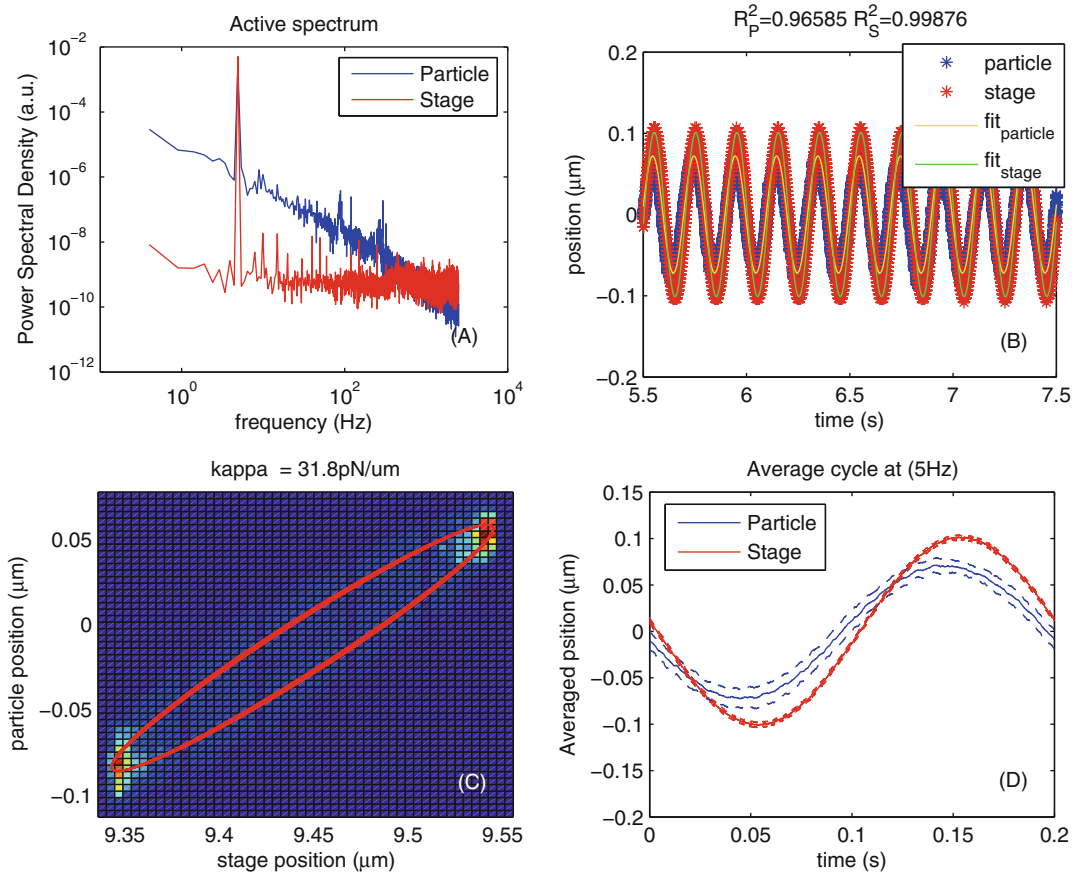

Fig. 10 Consistency checks for the active force calibration part. (**a**) Power spectra of particle and stage obtained during active calibration. The sharp frequency peak corresponds to the 5 Hz driving frequency in that particular active measurement. (**b**) Fragment of a time series showing the sinusoidal motion imposed by the stage during the experiment and corresponding response of the trapped granulus, with their respective sinusoidal fits. (**c**) Example showing the ellipsoidal shape corresponding to an undisturbed experiment where the trapped granulus follows the stage position with a phase-difference. (**d**) Illustration of the calculated average of all periods of the oscillation from the time series shown in (**b**). The sine wave reflecting the particle motion leads in phase relative to the sine wave corresponding to the stage motion. Even though counter intuitive, this result corresponds correctly to the situation in a non-inertial regime (low Reynolds number), where the particle position is driven by instantaneous forces, rather than responding to stage acceleration. The instantaneous forces are a combination of viscous and elastic forces. In a purely viscous media, the maximum of the particle position will correspond to the maximum of the stage speed. This point corresponds to the maximum derivative of the stage trajectory, which for a sinusoidal trajectory corresponds to the zero crossing point, just 90° before the stage maximum position. In a purely elastic medium (~solid) the force changes linearly with distance in respect to the equilibrium position, and the maximum in particle position is reached when the stage is at its maximum position, i.e., with a 0° phase difference with the stage. In a viscoelastic material on the other hand, the phase will be somewhere in between 90° and 0°, with the particle trajectory always being advanced with respect to the stage due to the viscous component, which is what we observe in (**d**). The individual panels in this figure were created using a custom-written MATLAB program that analyses the experimental recordings

(A) shows the power spectral density of both trapped particle and stage; confirming the driving frequency of 5 Hz and no other particular noise peaks. Panel (B) and (C) illustrate the sinusoidal behavior of both particle and stage, panel (C) shows indeed the elliptical shape mentioned in point (4) above. Finally, panel (D) presents the average of all oscillations and indicate the phase difference between particle and stage.

References

1. Fazal FM, Block SM (2011) Optical tweezers study life under tension. Nat Photonics 5:318–321
2. Moffitt JR, Chemla YR, Smith SB et al (2008) Recent advances in optical tweezers. Annu Rev Biochem 77(1):205–228
3. Greenleaf WJ, Woodside MT, Block SM (2007) High-resolution, single-molecule measurements of biomolecular motion. Annu Rev Biophys Biomol Struct 36:171–190
4. Neuman KC, Nagy A (2008) Single-molecule force spectroscopy: optical tweezers, magnetic tweezers and atomic force microscopy. Nat Methods 5(6):491–505
5. Berg-Sørensen K, Flyvbjerg H (2004) Power spectrum analysis for optical tweezers. Rev Sci Instrum 75(3):594–612
6. Tolić-Nørrelykke SF, Schäffer E, Howard J et al (2006) Calibration of optical tweezers with positional detection in the back focal plane. Rev Sci Instrum 77(10):103101
7. Neuman KC, Block SM (2004) Optical trapping. Rev Sci Instrum 75(9):2787–2809
8. Gittes F, Schmidt CF (1998) Signals and noise in micromechanical measurements. Methods Cell Biol 55:129–156
9. Veigel C, Schmidt CF (2011) Moving into the cell: single-molecule studies of molecular motors in complex environments. Nat Rev Mol Cell Biol 12(3):163–176
10. Sims PA, Xie XS (2009) Probing dynein and kinesin stepping with mechanical manipulation in a living cell. ChemPhysChem 10(9-10):1511–1516
11. Leidel C, Longoria RA, Gutierrez FM et al (2012) Measuring molecular motor forces in vivo: implications for tug-of-war models of bidirectional transport. Biophys J 103 (3):492–500
12. Shubeita GT, Tran SL, Xu J et al (2008) Consequences of motor copy number on the intracellular transport of kinesin-1-driven lipid droplets. Cell 135(6):1098–1107
13. Guet D, Mandal K, Pinot M et al (2014) Mechanical role of actin dynamics in the rheology of the Golgi complex and in Golgi-associated trafficking events. Curr Biol 24 (15):1700–1711
14. Oddershede LB (2012) Force probing of individual molecules inside the living cell is now a reality. Nat Chem Biol 8(11):879–886
15. Norregaard K, Jauffred L, Berg-Sorensen K et al (2014) Optical manipulation of single molecules in the living cell. Phys Chem Chem Phys 16(25):12614–12624
16. López-Quesada C, Fontaine AS, Farré A et al (2014) Artificially-induced organelles are optimal targets for optical trapping experiments in living cells. Biomed Opt Express 5 (7):1993–2008
17. Gross SP (2003) Application of optical traps in vivo. Methods Enzymol 361:162–174
18. Rasmussen MB, Oddershede LB, Siegumfeldt H (2008) Optical tweezers cause physiological damage to Escherichia coli and Listeria bacteria. Appl Environ Microbiol 74(8):2441–2446
19. Peterman EJG, Gittes F, Schmidt CF (2003) Laser-induced heating in optical traps. Biophys J 84(2):1308–1316
20. Neuman KC, Chadd EH, Liou GF et al (1999) Characterization of photodamage to Escherichia coli in optical traps. Biophys J 77 (5):2856–2863
21. Lee YJ, Patel D, Park S (2011) Local rheology of human neutrophils investigated using atomic force microscopy. Int J Biol Sci 7 (1):102–111
22. Wilhelm C (2008) Out-of-equilibrium microrheology inside living cells. Phys Rev Lett 101 (2):028101
23. Dufrene YF, Evans E, Engel A et al (2011) Five challenges to bringing single-molecule force spectroscopy into living cells. Nat Methods 8 (2):123–127
24. Jun Y, Tripathy SK, Narayanareddy BR et al (2014) Calibration of optical tweezers for

in vivo force measurements: how do different approaches compare? Biophys J 107 (6):1474–1484

25. Tolić-Nørrelykke IM, Munteanu E-L, Thon G et al (2004) Anomalous diffusion in living yeast cells. Phys Rev Lett 93(7):078102
26. Schnurr B, Gittes F, MacKintosh FC et al (1997) Determining microscopic viscoelasticity in flexible and semiflexible polymer networks from thermal fluctuations. Macromolecules 30(25):7781–7792
27. Gittes F, Schnurr B, Olmsted PD et al (1997) Microscopic viscoelasticity: shear moduli of soft materials determined from thermal fluctuations. Phys Rev Lett 79(17):3286–3289
28. Mas J, Farré A, López-Quesada C et al (2011) Measuring stall forces in vivo with optical tweezers through light momentum changes. Proc SPIE 8097:809726
29. Farré A, Montes-Usategui M (2010) A force detection technique for single-beam optical traps based on direct measurement of light momentum changes. Opt Express 18 (11):11955–11968
30. Farré A, Marsà F, Montes-Usategui M (2012) Optimized back-focal-plane interferometry directly measures forces of optically trapped particles. Opt Express 20(11):12270–12291
31. Smith SB, Cui Y, Bustamante C (2003) Optical-trap force transducer that operates by direct measurement of light momentum. In: Methods in Enzymology. Academic, New York, NY, pp 134–162
32. Hendricks AG, Holzbaur EL, Goldman YE (2012) Force measurements on cargoes in living cells reveal collective dynamics of microtubule motors. Proc Natl Acad Sci U S A 109 (45):18447–18452
33. Vermeulen KC, van Mameren J, Stienen GJM et al (2006) Calibrating bead displacements in optical tweezers using acousto-optic deflectors. Rev Sci Instrum 77(1):013704
34. Blehm BH, Schroer TA, Trybus KM et al (2013) In vivo optical trapping indicates kinesin's stall force is reduced by dynein during intracellular transport. Proc Natl Acad Sci 110 (9):3381–3386
35. Valentine MT, Guydosh NR, Gutiérrez-Medina B et al (2008) Precision steering of an optical trap by electro-optic deflection. Opt Lett 33(6):599–601
36. Mas J, Richardson AC, Reihani SN et al (2013) Quantitative determination of optical trapping strength and viscoelastic moduli inside living cells. Phys Biol 10(4):046006
37. Fischer M, Richardson AC, Reihani SN et al (2010) Active-passive calibration of optical tweezers in viscoelastic media. Rev Sci Instrum 81(1):015103
38. Fischer M, Berg-Sorensen K (2007) Calibration of trapping force and response function of optical tweezers in viscoelastic media. J Opt A Pure Appl Opt 9(8):S239–S250
39. Atakhorrami M, Sulkowska JI, Addas KM et al (2006) Correlated fluctuations of microparticles in viscoelastic solutions: Quantitative measurement of material properties by microrheology in the presence of optical traps. Phys Rev E 73(6):061501
40. Mizuno D, Head DA, MacKintosh FC et al (2008) Active and passive microrheology in equilibrium and nonequilibrium systems. Macromolecules 41(19):7194–7202
41. Lee H, Ferrer JM, Nakamura F et al (2010) Passive and active microrheology for cross-linked F-actin networks in vitro. Acta Biomater 6(4):1207–1218
42. Lau AWC, Hoffman BD, Davies A et al (2003) Microrheology, stress fluctuations, and active behavior of living cells. Phys Rev Lett 91 (19):198101
43. Robert D, Nguyen T-H, Gallet F et al (2010) In vivo determination of fluctuating forces during endosome trafficking using a combination of active and passive microrheology. PLoS One 5(4):e10046
44. Andersson M, Czerwinski F, Oddershede LB (2011) Optimizing active and passive calibration of optical tweezers. J Opt 13(4):044020
45. Oddershede L, Greco S, Nørrelykke SF et al (2001) Optical tweezers: probing biological surfaces. Probe Microsc 2:129
46. Gittes F, Schmidt CF (1998) Interference model for back-focal-plane displacement detection in optical tweezers. Opt Lett 23(1):7–9
47. Pralle A, Prummer M, Florin EL et al (1999) Three-dimensional high-resolution particle tracking for optical tweezers by forward scattered light. Microsc Res Tech 44(5):378–386
48. Leijnse N, Jeon JH, Loft S et al (2012) Diffusion inside living human cells. Eur Phys J Spec Top 204(1):75–84
49. Dreyer JK, Berg-Sorensen K, Oddershede L (2004) Improved axial position detection in optical tweezers measurements. Appl Opt 43 (10):1991–1995
50. Richardson AC, Reihani SNS, Oddershede LB (2008) Non-harmonic potential of a single beam optical trap. Opt Express 16 (20):15709–15717
51. Mizuno D, Tardin C, Schmidt CF et al (2007) Nonequilibrium mechanics of active cytoskeletal networks. Science 315(5810):370–373

52. Mizuno D, Bacabac R, Tardin C et al (2009) High-resolution probing of cellular force transmission. Phys Rev Lett 102(16):168102
53. Ott D, Reihani SN, Oddershede LB (2014) Crosstalk elimination in the detection of dual-beam optical tweezers by spatial filtering. Rev Sci Instrum 85(5):053108
54. Jeon J-H, Tejedor V, Burov S et al (2011) In vivo anomalous diffusion and weak ergodicity breaking of lipid granules. Phys Rev Lett 106 (4):048103
55. Selhuber-Unkel C, Yde P, Berg-Sorensen K et al (2009) Variety in intracellular diffusion during the cell cycle. Phys Biol 6(2):025015
56. Yamada S, Wirtz D, Kuo SC (2000) Mechanics of living cells measured by laser tracking microrheology. Biophys J 78(4):1736–1747
57. Wei M-T, Zaorski A, Yalcin HC et al (2008) A comparative study of living cell micromechanical properties by oscillatory optical tweezers. Opt Express 16(12):8594–8603
58. Czerwinski F, Richardson AC, Oddershede LB (2009) Quantifying noise in optical tweezers by allan variance. Opt Express 17(15): 13255–13269